Article

Exploring the Potential of SCOPE Model for Detection of Leaf Area Index and Sun-Induced Fluorescence of Peatland Canopy

Anshu Rastogi [1,2,*], Michal Antala [1], Egor Prikaziuk [2], Peiqi Yang [2,3], Christiaan van der Tol [2] and Radoslaw Juszczak [1]

1 Laboratory of Bioclimatology, Department of Ecology and Environmental Protection, Faculty of Environmental Engineering and Mechanical Engineering, Poznan University of Life Sciences, Piątkowska 94, 60-649 Poznan, Poland
2 Faculty of Geo-Information Science and Earth Observation (ITC), University of Twente, 7500 AE Enschede, The Netherlands
3 School of Geography, Nanjing Normal University, Nanjing 210097, China
* Correspondence: anshu.rastogi@up.poznan.pl; Tel.: +48-618466551

Abstract: The study of peatland is challenging due to the water saturation and evergreen mixed vegetation that ranges from simple forms of plants such as mosses to higher forms of plants such as cranberries, grasses, etc. The changing water level through the growing season makes the peatland vegetation very dynamic. In this work, we have used ground-level remote-sensing signals to understand the dynamic nature of peatland vegetation. We have also estimated the leaf area index (LAI) and Sun-Induced fluorescence (SIF) through the Soil Canopy Observation of Photosynthesis and Energy fluxes (SCOPE) model. The estimated LAI and SIF were compared with the Normalized Difference Vegetation Index (NDVI), Enhanced Vegetation Index (EVI), Near-Infrared Reflectance of vegetation (NIRv), and measured SIF. The modeled LAI was observed to be significantly correlated with NDVI, EVI, and NIRv, whereas a good correlation was observed between measured and modeled SIF. Along with showing the dynamic behavior of peatland vegetation, the study indicates that SCOPE in its inverted form can be used to estimate reflectance-based LAI for peatland, which can be more reliable to present biomass and productivity of peatland ecosystem in comparison to transmittance-based LAI measurement for such ecosystem. The good correlation between measured and modeled SIF at 760 nm indicates that a reliable SIF value can be estimated through the SCOPE model for a complex ecosystem such as peatland, which can be very helpful in the absence of high-resolution hyperspectral data (usually used for SIF measurements).

Keywords: sun-induced fluorescence; leaf area index; peatland; radiative transfer model; vegetation indices

1. Introduction

Peatlands cover around 3% of terrestrial area but contain around 30% of terrestrial carbon [1]; therefore, the peatlands have the potential for strong feedback on the global climate system, but their response to future climatic conditions is highly uncertain [2–4]. The dynamics of peatlands are considered to be nonlinear, which may consist of long periods of stasis punctuated by occasional abrupt shifts to totally different regimes [5]. Thus, the peatlands, which at present act as a carbon sink, may act as a source of carbon with the future changes in climatic conditions. Therefore, monitoring peatland vegetation is needed to have an idea about this ecosystem in a rapidly changing environment. The observation of peatland vegetation directly by personal surveys and measurements is tedious and time-consuming. Therefore, remote sensing, especially satellite remote sensing is an appreciated alternative approach for vegetation assessment. [6]. However, for a better understanding of remote-sensing signals obtained through satellites, there is a need to perform studies at the ground level. In recent times, several studies have been performed

on peatland using remote-sensing techniques reviewed in Chasmer et al. [7]. Different reflectance-based vegetation indices (VIs) are commonly used to monitor vegetation at satellite or ground scales. Some of the most commonly used VIs are Normalized Difference Vegetation Index (NDVI), Simple Ratio (SR), Photochemical Reflectance Index (PRI), and Enhanced Vegetation Index (EVI) [8,9]. Many more indices/signals have been developed over decades, and recently indices/signals such as Near-Infrared Reflectance of vegetation (NIRv) and Sun Induced Fluorescence (SIF) aim to assess the photosynthetic activity of plants [10–12]. The reflectance-based indices are connected to photosynthetic activity only indirectly, and the changes in the physiological status of plants are apparent after some time when structural changes appear in plants. The Fluorescence Correction Vegetation Index (FCVI) was developed to consider the structural changes for a more precise measurement of photosynthetic activity in combination with SIF [13]. In the last decade, due to the availability of a high number of spectral bands and resolutions, hyperspectral remote sensing has been used to understand the vegetation properties of peatlands [14–17]. In peatland, the vegetation properties and structure are changing rapidly. A period of warm weather without rain causes mosses to dry, whereas vascular plants continue to grow due to high groundwater levels. This changes rapidly after the rain when the mosses start to become green. The dynamic phenomena occurring in peatland lead to remote sensing signals that need to be explained differently compared to croplands or ecosystems made of similar vegetation groups. To understand the dynamic behavior of peatland, a dedicated field experiment was designed in Poland [3,18]. The vegetation coverage and its structural properties play an important role in the understanding of light interaction; therefore, along with vegetation indices, the canopy-leaf area index (LAI) is often used for the estimation of plant productivity and biomass. Even if the LAI is an important factor for ecosystem understanding, its measurement/estimation is not easy due to spatial and temporal heterogeneity. Several methods to measure or estimate LAI are available [19]. Direct methods are the most accurate but tedious and time-consuming and can be destructive, whereas ground-based methods of LAI measurements are based on radiation transmittance, and remote-sensing methods are based on reflectance. For an ecosystem like peatland, the exact measurement of transmittance is impossible due to the presence of mosses attached to the ground; therefore, the ground-based method can only be used to estimate the vascular plants' LAI and are of limited use. The reflectance-based remote-sensing method of LAI estimation can more correctly represent the ecosystem behavior as it also includes the LAI of non-vascular plants.

The biochemical composition of vegetation and its structure directly influence vegetation's absorption and reabsorption properties. The radiative transfer models (RTMs) of vegetation are tools to explain the light interaction with leaves and vegetation canopies. The interaction of radiation with leaves' internal structure is responsible for important physiological processes in the plant, such as photosynthesis and transpiration. Thus, the light-leaf interaction determines the exchange of energy and matter between vegetation and the atmosphere. Therefore, the RTMs are used to connect the vegetation properties with remote-sensing observations and vegetation monitoring. However, the application of RTMs is challenging because of the unavailability of all the required parameters to feed into the RTMs. By inverting a coupled RTM-photosynthesis model to hyperspectral proximal sensing (reflectance and SIF), the properties of vegetation can be analyzed and can be further used in RTMs to retrieve the photosynthetic properties and energy balance of vegetation [20–22]. Soil Canopy Observation of Photosynthesis and Energy fluxes (SCOPE) is one of the RTMs that incorporates different models to understand radiation within vegetation canopies [23]. Even after certain limitations in SCOPE, such as not having soil water balance and consideration of leaves clumping, the model has proven to be robust for the study of several vegetations and their functioning [23–25]. The implementation of the SCOPE model for the purpose of understanding certain characteristics of peatland vegetation has not been undertaken before. Therefore, the objectives of this work are (1) to decipher the potential of SCOPE inversion in the simulation of LAI for peatland vegetation.

(2) to observe the potential of SCOPE for SIF estimation of the peatland ecosystem when the high-resolution hyperspectral sensors for fluorescence spectrum retrieval are not available.

2. Material and Method

2.1. Experimental Site

The field experiment was conducted in Rzecin peatland (52°45′41″N, 16°18′35″E). The vegetation found in this site is very heterogenous with a clear gradient of rich-poor fen vegetations, where rich fen vegetations dominated by vascular plants are found near the edge, and the poor fen vegetations, rich in bryophytes, are present in the middle of the ecosystem [26]. There are two climate manipulation sites developed in poor fen peatland areas, which are 50 m away from each other, but significantly different in vegetation due to their varying water table depth dynamics [18]. The CL site is the site dominated by *Carex lasiocarpa,* whereas the CR site is dominated by *Carex rostrata* among vascular plants. The sites are further divided into plots with different microclimates, where the microclimate is being manipulated to raise temperatures by the use of open-top chambers, infrared heaters, and rain curtains. The plots are randomly distributed within the sites with three repetitions, where the plots without manipulation are control (C) plots, with open-top chambers and heaters are warming (W) plots, whereas the plots with night-time reduction in the rain, open-top chambers, and heaters are warming and reduced precipitation (WP) plots (Figure 1). The manipulation sites were developed in 2017 and described in Górecki et al. [18]. Górecki et al. [18] also describe all the infrastructure and routine measurements that are being performed at the manipulation site at regular intervals, such as water pH, water conductivity, nutrient content of water, vegetation chlorophyll, its abundance, morphological characteristic etc. The 100 W heaters were added in March 2021 to increase the night-time temperature of the manipulated plots. The measurements used in this study were collected during the growing season of 2021.
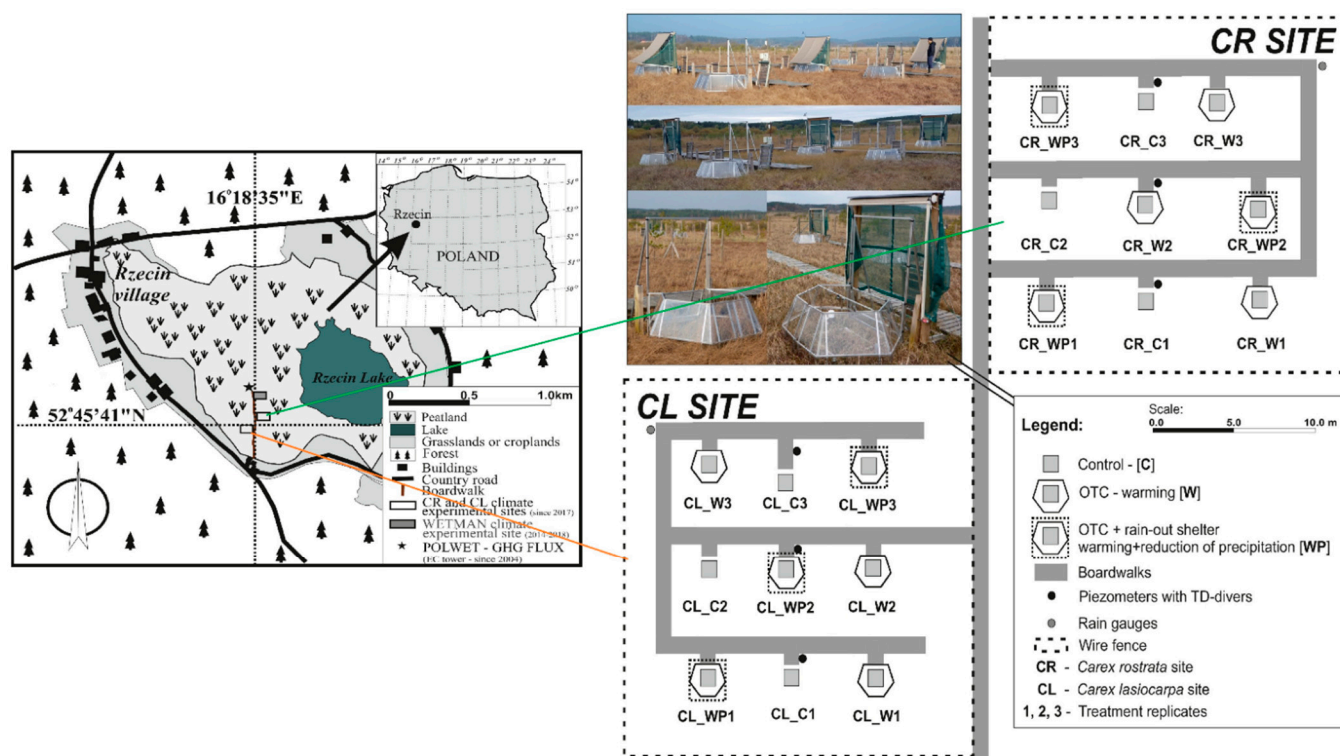

Figure 1. Shows the location of Rzecin peatland where CL and CR represent the climate manipulation sites (Adopted from Górecki et al. [18], CC BY-NC-ND license).

2.2. Measurement of Hyperspectral and Vegetation Properties

The top of canopy (TOC) spectra were collected periodically (around noontime, under clear sky conditions, from nadir position) through the hyperspectral system Piccolo Doppio [27]. This system has a Dual Field Of View (DFOV) with cosine corrected foreoptics to capture down-welling irradiance and the upwelling radiance. In the system, a double bifurcated fiber optic is used to transfer light from the foreoptics to the spectrometers; therefore, each spectrometer receives light from the same Earth surface area (each measurement has the same footprint, which is critical for the accuracy of reflectance and SIF estimations and their relationships). The system consists of two hyperspectral spectrometers; the first is FLAME-T-VIS_NOR of Ocean Optics, Dunedin, FL, USA (Spectral range 400–1000 nm; with a full-width half maximum "FWHM" 1.3 nm) from where the spectra were collected to calculate VIs shown in Table 1. The second spectrometer is the QEProFL Spectrometer (Spectral range 640–780 nm, with FWHM 0.31 nm) of Ocean Optics USA, designed to measure the spectral region, which contains the O_2-A and O_2-B bands to calculate SIF at both peaks of 740 nm and 680 nm. The SIF was calculated with the improved Fraunhofer Line Depth (iFLD) methods (as described in Alonso et al. [28]). Three replicates in three technical replicates (i.e., a total of 9 spectra from 3 points within each plot) were measured from the nadir position, where upwelling optics was approximately at 1.4 m above the peat surface with a field of view of 0.62 m. Per point 5 spectra were collected, where the first and last spectra were for dark current (with a closed optical shutter), whereas the middle three spectra were collected with an open shutter. The irradiance and radiance were calculated after subtracting the dark current and applying the calibration factor provided by National Institute for Laser, Plasma and Radiation Physics (NIFLPR), Romania. The reflectance spectra were calculated by dividing radiance by irradiance, and an average of nine spectra from each plot was calculated to minimize the noise and used for modeling purposes.

Table 1. Spectral vegetation indices calculated from ground-based spectroscopy (ρ–reflectance at a given wavelength; NDVI is Normalized Difference Vegetation Index; EVI is Enhanced Vegetation Index, and NIRv is Near-Infrared Reflectance of vegetation.

Vegetation Indices	Formula	References
NDVI	$\dfrac{\rho860-\rho670}{\rho860+\rho670}$	[29]
EVI	$2.5\left[\dfrac{(\rho860-\rho670)}{(\rho860)+6(\rho670)-7.5(\rho480)+1}\right]$	[30]
NIRv	$\rho860\dfrac{\rho860-\rho670}{\rho860+\rho670}$	[9]

The LAI was non-destructively estimated from each plot using a widely used SunScan plant-canopy analyzer system (Delta-T, Burwell, UK). The LAI used here represents a one-sided leaf area divided by a unit of horizontal surface area. The protocol followed for the measurement is described in Rastogi et al. [31]. LAI measured through SunScan represents the plant area index (PAI) of vascular plants. There was no way to measure mosses LAI through this instrument, whereas differentiation of non-green and green LAI was also not possible by using only the SunScan device. Due to the malfunction of SunScan in October, the measurements were taken only till September 2021.

The CCM 300 (OPTI-SCIENCES, Hudson, NH, USA) device was used to measure the chlorophyll content of different species on different plots and sites. The data was not directly used as the plant distribution was different in different plots, but it provided the idea of the expected range of chlorophyll content of peatland vegetation for different species.

2.3. Implementation of SCOPE

We first used the codes for SCOPE inversion to retrieve biophysical and biochemical parameters of the peatland vegetation [20,32]. The inversion was performed through a numerical optimization algorithm where the measured reflectance between 400 to 900 nm is fitted to get the best fit for the modeled apparent reflectance.

An example of the spectral fitting obtained is shown in Figure 2. The principle behind SCOPE retrieval is described in Van der Tol et al. [20] and extended by Celesti et al. [21]. As our ecosystem is an evergreen ecosystem due to the presence of Sphagnum and *Oxycoccus palustris*, the chlorophyll concentration for the canopy can never be zero. Therefore, we set up the lower boundary for chlorophyll to be 5 µg cm^{-2}, whereas the upper boundary was set to 40 µg cm^{-2} (the ecosystem is nutrient-poor, and our ground measurements showed we can never cross this value). The lower and upper boundaries and initialization values for different parameters are indicated in Table 2. The solar-zenith angle from each campaign was used, whereas the Full Width at Half Maximum (FWHM) for the FLAME spectrometer was 1.3 nm. All the parameters were left free to vary during the application of SCOPE inversion. A fit of modeled reflectance spectra was observed with the measured one (the spectral fit is shown in Figure 2). The obtained parameter from SCOPE inversion was combined with data such as radiance, temperature, humidity, and zenith angle to run the SCOPE forward model.
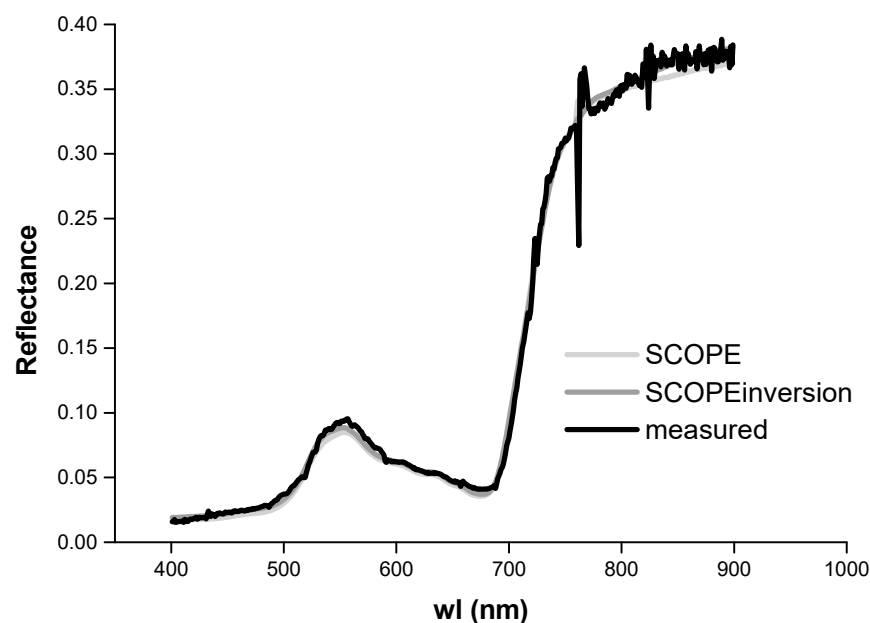

Figure 2. Representative reflectance spectra from a plot showing the fitting of reflectance obtained by SCOPE inversion and SCOPE to the measured reflectance spectrum in the range of 400 to 900 nm of wavelength (wl).

Table 2. Parameters variability applied in Soil Canopy Observation of Photosynthesis and Energy fluxes inversion.

Parameters	Unit	Lower Boundary	Upper Boundary	Initial Value
Soil brightness (B)	-	0	0.9	0.89
Spectral shape latitude (lat)	-	20	40	40
Spectral shape longitude (lon)	-	40	60	40
Soil moisture volume percentage (smp)	%	5	80	50
Chlorophyll content (Cab)	µg cm^{-2}	5	40	15
Dry matter content (Cdm)	g cm^{-2}	0.00	0.02	0.007
Leaf water thickness equivalent (Cw)	cm	0	0.2	0.080
Senescent material (Cs)	fraction	0	0.4	0.114
Carotenoids content (Cca)	µg cm^{-2}	0	25	8.381
Anthocyanin content (Cant)	µg cm^{-2}	0	40	1.4
Leaf structure parameter (N)	-	1	3.5	1.5
Leaf area index (LAI)	m^2 m^{-2}	0.1	5	2
Leaf inclination (lidfa)	-	−1	1	−0.3
Leaf inclination bimodality (lidfb)	-	−1	1	−0.114

2.4. Statistical Analysis

The significance of differences in VIs and measured and modeled LAI caused by manipulation were tested by one-way analysis of variance (ANOVA) for every measurement day and each site separately. The *t*-test was performed to investigate the significance of differences between two sites for each day separately. Coefficients of determination (r^2) for each couple of variables as well as root mean square error (RMSE) for modeled and measured SIF were derived from linear regression. All statistical analysis was performed in RStudio version 2022.02.0+443 (RStudio Inc., Boston, MA, USA).

3. Results

3.1. Measured LAI

The measured LAI shows a considerable variability and fluctuating pattern (Figures 3 and 4). The measured LAI values in February were observed to be higher than the measured LAI value in April for Cl and CR sites. The two-time measurements in May (10 May and 31 May) showed a fluctuation, whereas, from June, the measured LAI value was observed to be increasing for both the sites until the last measurement was taken in September 2021. A non-significant difference in measured LAI between the control and the manipulated plot was observed during the growing months of June, July, and August, where the warmer plots were observed to have higher LAI in comparison to control plots.

3.2. Vegetation Indices

NDVI was observed to be almost stable till April, whereas it started to increase in May, reached its peak in July, and then decreased till the measurement was conducted in October (Figures 3 and 4). For the CL site, the NDVI value got saturated around the peak of the vegetation season, i.e., in July and August, when the NDVI values reached around 0.85 (Figure 3). In CL, the manipulated plots show a slight increase in NDVI before it reached the saturating value (i.e., May and June), whereas for CR the slight increase in NDVI was observed for manipulated plots during the growing season. EVI and NIRv showed a very strong correlation in between for peatland vegetation over the whole vegetation season (Figure 5), although EVI takes higher values than NIRv (Figures 3 and 4). For EVI and NIRv, the manipulated plots were observed to have a slightly higher value than the control plots during the growing season.

3.3. Modeled LAI

The modeled LAI obtained through the inversion of the SCOPE model showed a clear seasonal pattern, where the value of LAI started to increase with each measurement until it reached its peak in July. After that, it tends to decrease towards its starting value for both sites. The modeled LAI of CR vegetation is steadily increasing from the end of February till its peak in July, while the modeled LAI of CL vegetation increased moderately till the middle of May and then more steeply till the peak in July. There were no statistically significant differences among treatments for any day of measurement, except modeled LAI on 16 June for CR vegetation (Supplementary Table S1), when LAI of W is significantly higher than LAI of C (*p*-value = 0.0258).

The differences between the two vegetation types (CL and CR) were observed to be significant only around the peak of the season (i.e., summer; Supplementary Table S2).

The correlation of measured LAI with modeled LAI and discussed VIs was observed to be weak (Figure 5). In contrast, the modeled LAI was well correlated with all examined green biomass-related VIs (NDVI, EVI, NIRv; Figure 5).
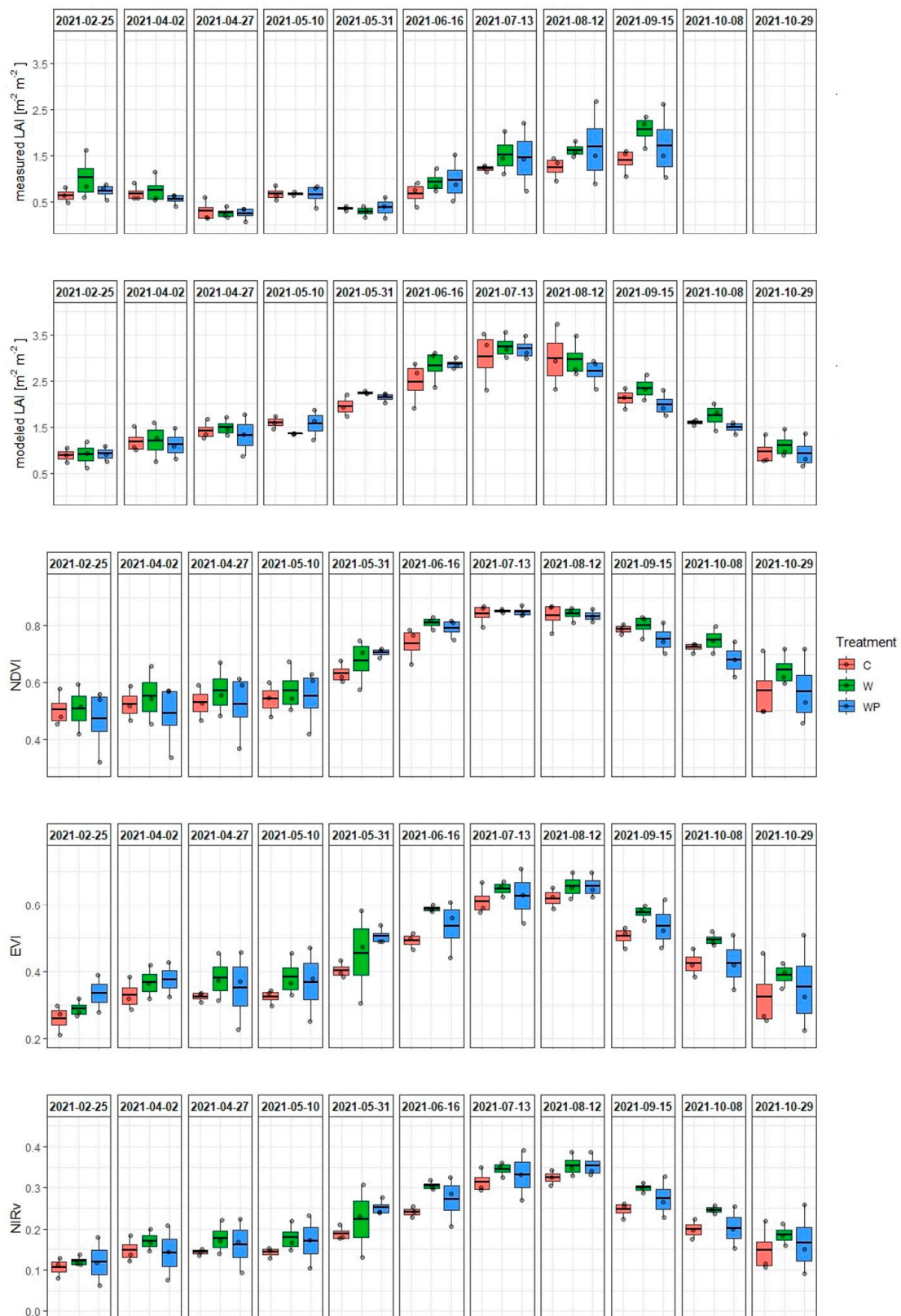
Figure 3. The changes in measured and modeled Leaf Area Index (LAI) along with Normalized Difference Vegetation Index (NDVI), Enhanced Vegetation Index (EVI), and near-infrared reflectance of vegetation (NIRv) for CL climate manipulation site at a different time in the year of 2021. C is for the control plot, W is for warming plots, and WP represents the warming and reduced precipitation plot.
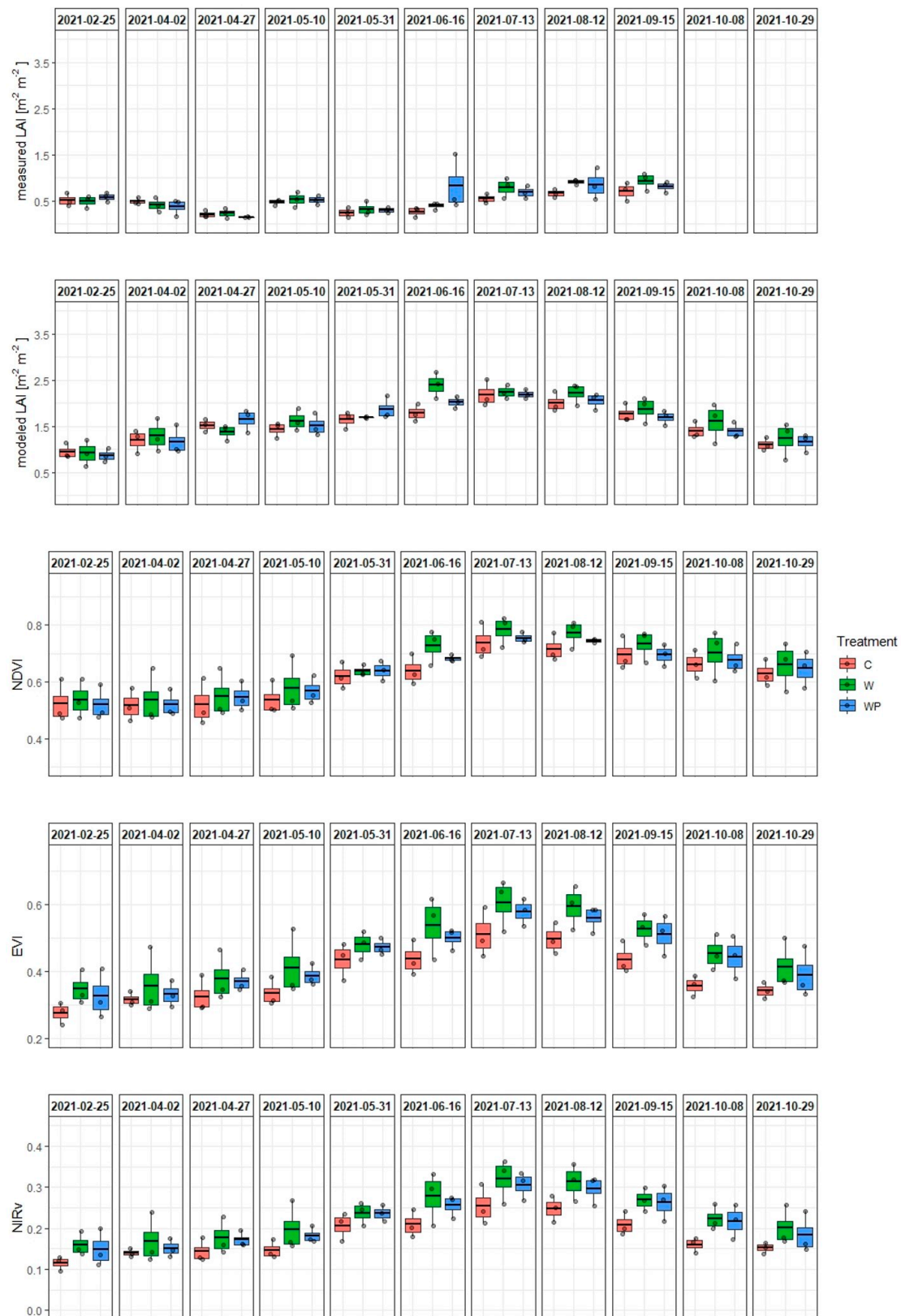
Figure 4. The changes in measured and modeled Leaf Area Index (LAI) along with Normalized Difference Vegetation Index (NDVI), Enhanced Vegetation Index (EVI), and near-infrared reflectance of vegetation (NIRv) for CR climate manipulation site at a different time in the year of 2021. C is for the control plot, W is for warming plots, and WP represents the warming and reduced precipitation plot.
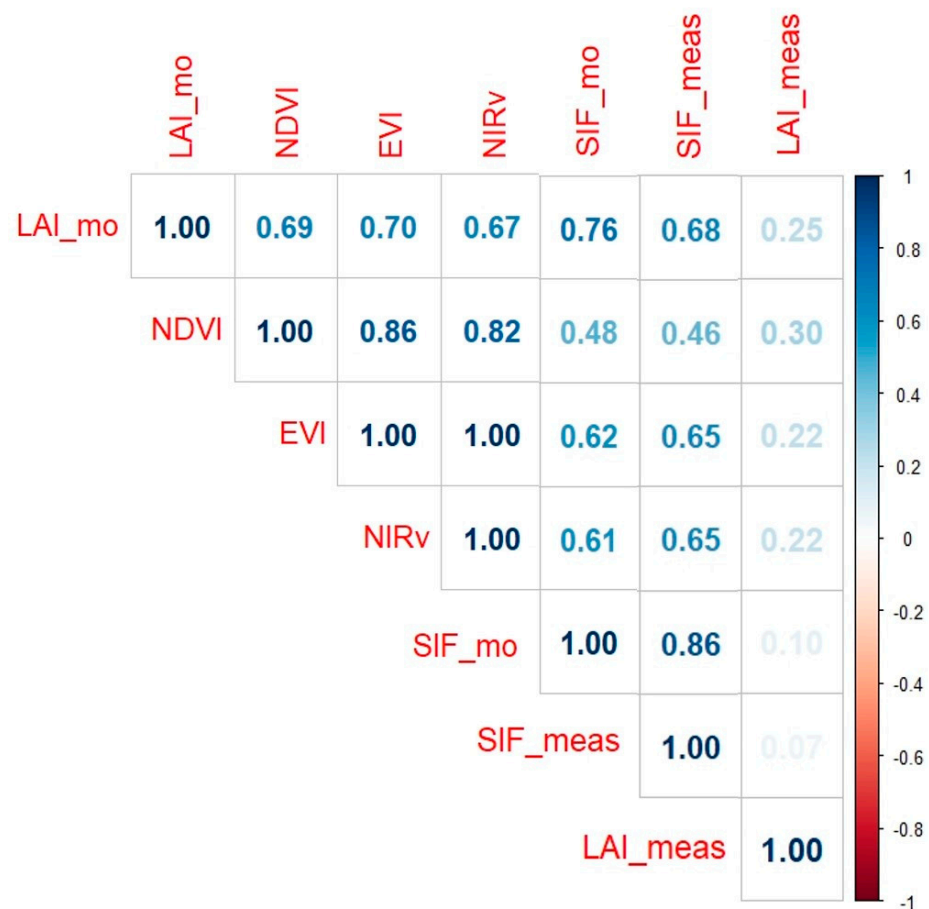
Figure 5. Correlations of modeled leaf area index (LAI_mo), Normalize Difference Vegetation Index (NDVI), Enhanced Vegetation Index (EVI), Near-Infrared Reflectance of vegetation (NIRv), modeled Sun-Induced Fluorescence (SIF_mo), measured Sun-Induced Fluorescence (SIF_meas), and measured leaf area index (LAI_meas) for both types of vegetation and all plots combined. Numbers represent r^2 for every couple.

3.4. Measured and Modeled SIF

Based on the retrieved plant traits and weather parameters, the SIF at 760 nm was modeled through the SCOPE and compared with the measured SIF at 760 nm (Figure 6). The measured and modeled SIF showed a clear seasonal pattern, where the SIF value started to increase in February, reaching the peak in July, and again showed a decrease in October. The differences in the SIF value of the CR site were more significant for manipulation than in the CL site, whereas the value of SIF in the CL site was higher during the growing season. The modeled SIF value kept a similar pattern as the measured SIF throughout the year. The modeled SIF was observed to be underestimated, but it showed a significant correlation with measured SIF with an R^2 of 0.86, where the correlation was performed for all the measurements on two sites for the year (Figure 7).
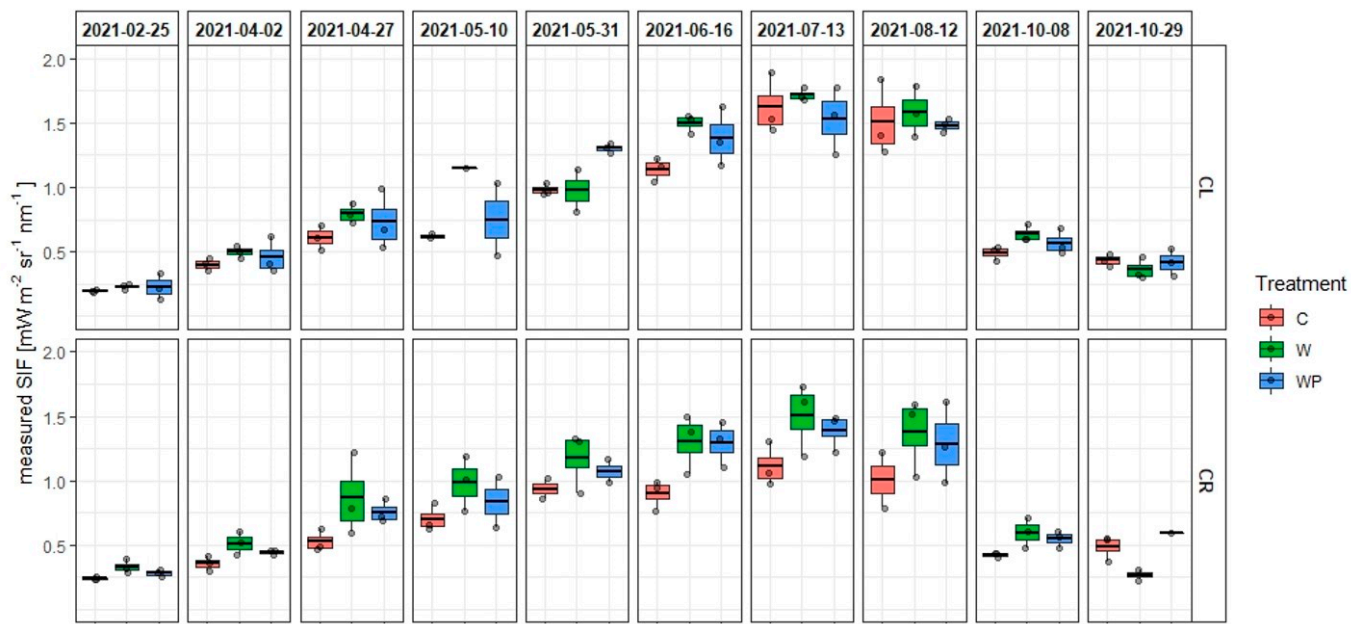
(**A**)
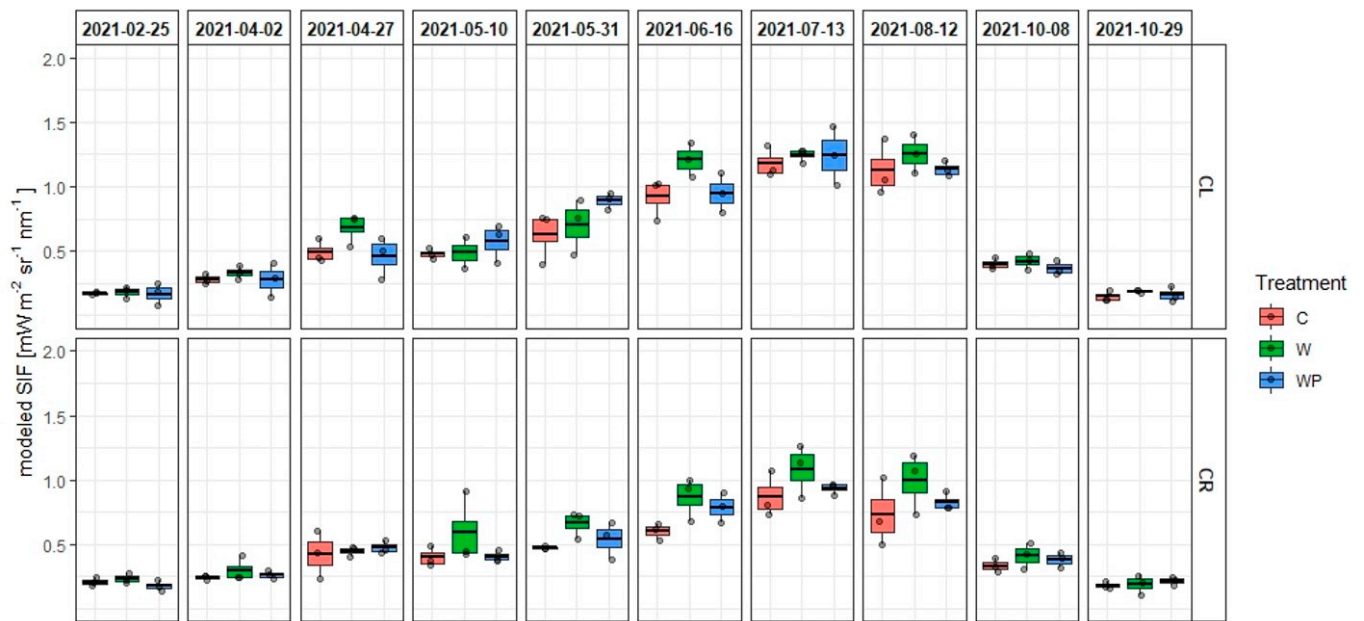
(**B**)

Figure 6. The changes in measured (**A**) and modeled (**B**) Sun-Induced Fluorescence (SIF) at 780 nm for CL and CR climate manipulation sites at a different time in the year 2021. C is for control plots, W is for warming plots, and WP represents warming and reduced-precipitation plots.
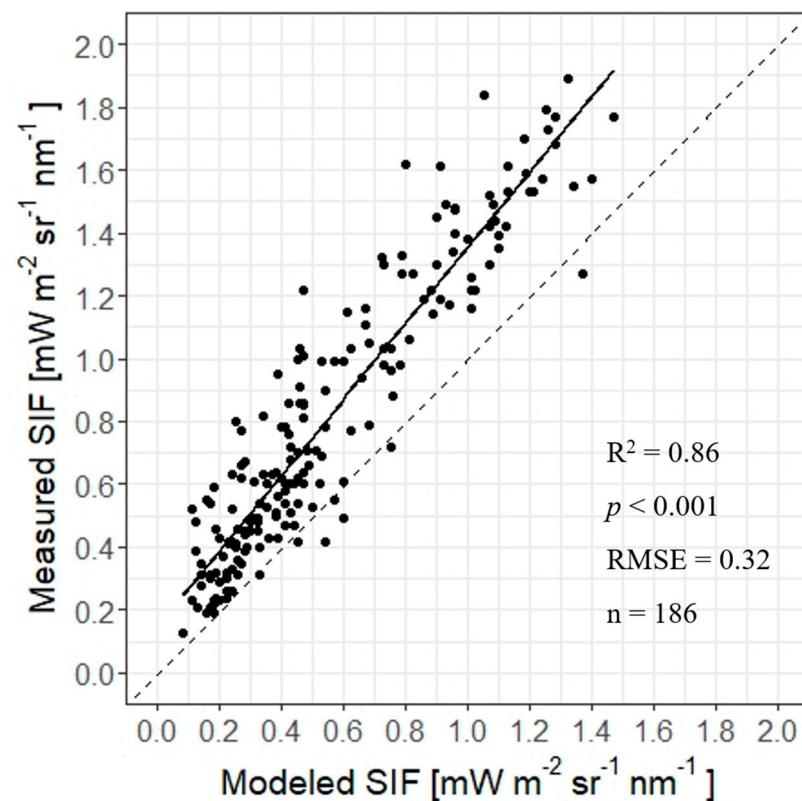
Figure 7. A comparison between measured and modeled Sun-induced fluorescence (SIF). The dashed line represents the theoretical ideal performance of the model.

4. Discussion

LAI is an important input in the model of several ecosystems for the purpose of predicting productivity and biomass; thus, it is important to correctly estimate the LAI [33,34]. The LAI estimation for an ecosystem such as peatland is complicated, as there is always a layer of mosses and slow decaying litter. In this work, the measured LAI, which represents the PAI of the vascular plant, does not correlate with modeled LAI. The decomposition process in peatland is slow [18], and a significant amount of litter was present at the beginning of the measurement, especially for the CL site, where the proportion of vascular plants is significantly higher (Figure 8). Therefore, after the winter, due to partial decomposition and no new biomass formation, the measured LAI was decreasing for the next few months before the vascular plants started to grow and contributed to the total measured LAI. As the biomass once created gets dry but remains on the plot, the measured LAI reaches a peak and then shows almost a stable pattern till September. On the contrary, modeled LAI showed a clear seasonal pattern, where the increase in LAI in March and April is mostly due to the contribution from mosses which are getting greener, whereas, from May, the vascular plants also start to grow and significantly contribute to the modeled LAI [35]. There is less proportion of Carex spp. in CR in relation to *Sphagnum* spp. and *Oxycoccus palustris*, whereas in the CL site, the proportion of *Carex* spp. is higher. The less biomass of *Carex* spp. means lower measured LAI; therefore, the difference between measured and modeled LAI is more than 100% for the CR site. The LAI values are high for CL, but the differences between measured and modeled LAI were observed to be lower for CL than for the CR site. This data can be easily understood when we consider the contribution of signals from mosses along with vascular plants for modeled LAI, whereas measured LAI considered vascular plants only. The observation indicates that measured LAI from the SunScan probe (DELTA-T, Burwell, UK) and modeled LAI are two different kinds of values (transmission and reflectance-based LAI estimation), especially for peatland. Measured LAI has significant value only when we are estimating the properties of vascular plants.

For the overall biomass and productivity analysis, modeled LAI might be more important, as it includes biomass of vascular and non-vascular plants, and it should be considered for peatlands. Thus, for the same reason, we used the modeled LAI value for the estimation of SIF through the SCOPE model.
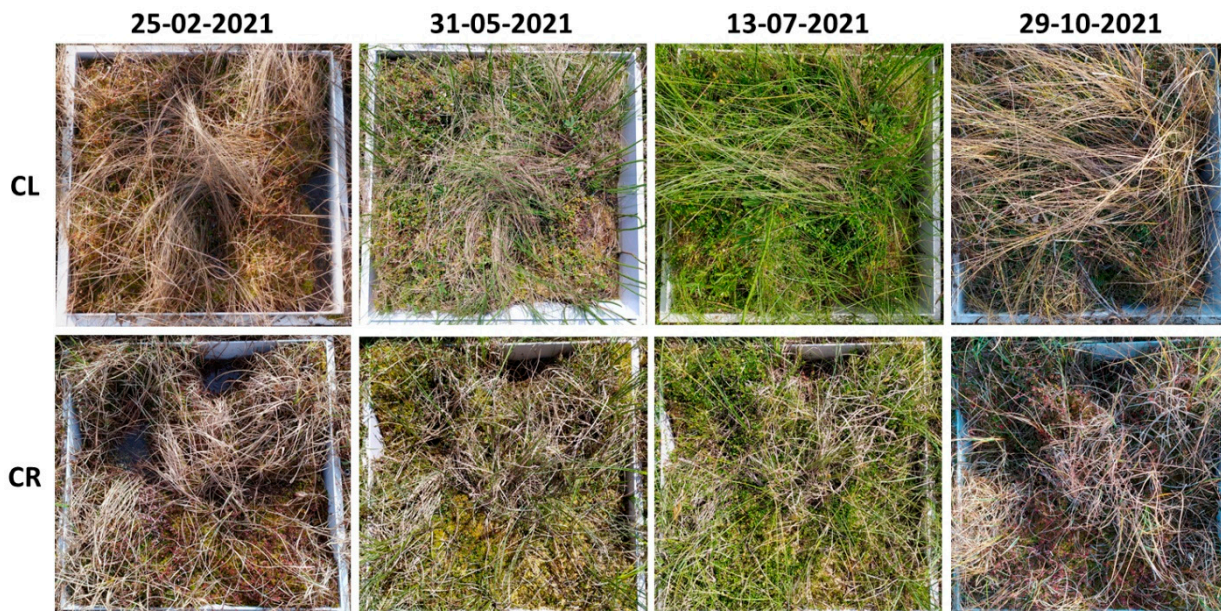

Figure 8. A representative picture of the control plot showing the seasonal dynamic of peatland vegetation at CL and CR sites.

The observation of various VIs is considered an efficient method for detecting the changes in the plant physiology at the ecosystem level, but VIs have their limitations; therefore, other indices such as SIF have been developed that can better present the physiological status of the vegetations [15,36]. In this study, NDVI, EVI, and NIRv showed a seasonal pattern for both the studied sites and was observed to be highly correlated with modeled LAI, but the correlation with measured LAI was observed to be poor (Figure 5), which can be again explained through the non-consideration of mosses and part of the litter interference in measured LAI. The NDVI gets saturated in July and August at the CL site (due to high LAI indicating higher biomass. Figures 3 and 4). This property of NDVI is well known and has contributed to red spectrum consideration, which reaches its peak with high LAI in the growing season [37], whereas the EVI and NIRv are considered to be more sensitive to canopy variation in comparison to NDVI [38]. NIRv is a relatively new index that is considered to be more correlated with SIF and GPP at specific temporal scales [9], but still, its interpretation is debated due to several facts, such as the consideration of spectrum band related to fAPAR estimation, its linear correlation with NIR, etc. [39]. Interestingly EVI and NIRv have shown a very similar pattern in this study with a correlation of 1. For the manipulation sites, the variation in VIs was observed, but the differences between the treatments were non-significant for most of the cases, indicating the need for more data collection, including the vegetation composition data. Whereas the differences in VIs and LAI between CL and CR during the summer were observed to be significant, indicating the importance of hydrological regimes and fluctuations of water table depth for peatland vegetation (Supplementary Table S2) [18].

All the studied VIs showed a slow increase and decrease in their value, whereas the SIF was observed to increase slowly but showed a sharp decrease in its value in October. SIF is dependent on three factors: light absorption, SIF reabsorption and scattering, and the relation between photosynthesis and Non-Photochemical Quenching (NPQ), which is nonlinear [15]. The temperature is decreasing rapidly in October, which significantly impacts the photosynthetic activity. Lower light intensity results in a lower amount of

absorbed energy (in comparison to previous months), most of which goes to photosynthesis and NPQ in colder conditions [40], whereas higher biomass increases the scattering of SIF in the far-red region, which may result in a significant decrease in SIF 760 value as observed at the top of the canopy. The SIF signal is a relatively new signal that needs high-resolution hyperspectral sensors, complex processing, and several other logistic and financial limitations like other new sensors, limiting the available data. The retrieval of SIF is still in its developing stage, and the number of experts to understand and retrieve these signals is limited although increasing. Like all new sensors in their initial phase, the SIF measuring instruments are comparatively expansive in respect to several remote-sensing devices used for reflectance collection and vegetation characterization through VIs. Thus, people are trying several ways to estimate SIF through the existing remote-sensing methods [10–12]. RTM is one of the methods widely used to estimate vegetation properties in the remote-sensing field. SCOPE is a widely accepted canopy model for the purpose of SIF retrieval [22–24]. Our observation indicated the SCOPE retrieved SIF, i.e., modeled SIF (even if slightly underestimated), correlated well with the measured SIF for a complex ecosystem like peatland, indicating the robust nature of SCOPE for the retrieval of SIF signals.

5. Conclusions

This study showed that the SCOPE in its inverted form can be used to retrieve the vegetation traits such as LAI for peatland vegetation, which is not easy to measure through traditional methods such as SunScan, whereas the SIF retrieved through SCOPE correlates well with measured SIF, indicating the possibility of using the SCOPE model for the purpose of retrieving SIF from peatland vegetation. Along with the application of the SCOPE, this is the first time we have shown the whole growing year spectral data along with SIF and LAI for peatland vegetation.

Supplementary Materials: The following supporting information can be downloaded at: https://www.mdpi.com/article/10.3390/rs14164010/s1. Table S1: *p*-values of one-way analysis of variance for modeled leaf area index (LAI_mo), Normalize Difference Vegetation Index (NDVI), Enhanced Vegetation Index (EVI), Near-Infrared Reflectance of vegetation (NIRv), and measured leaf area index (LAI_meas) in every day of measurements. The bold values present the statistically significant differences between treatments (control, warming, and warming and reduced precipitation) at alpha < 0.05. Table S2: *p*-values of t-test between CL and CR vegetation in every day of measurements. The bold values present the statistically significant differences between treatments at alpha < 0.05

Author Contributions: A.R.: Conceptualization, collection of data, Formal analysis, Investigation, Funding acquisition, Preparation of first draft; M.A.: Collection of data, Analysis, editing; E.P.: Analysis, review and editing; P.Y.: Analysis, review and editing; C.v.d.T.: Supervision, Review and editing; R.J.: Experimental design, Conceptualization, management, Review and editing, Funding acquisition. All authors have read and agreed to the published version of the manuscript.

Data Availability Statement: Readers can obtain the datasets through request to corresponding author.

Conflicts of Interest: The authors declare no conflict of interest.

References

1. Gorham, E. Northern peatlands: Role in the carbon cycle and probable responses to climatic warming. *Ecol. Appl.* **1991**, *1*, 182–195. [CrossRef] [PubMed]
2. Samson, M.; Słowińska, S.; Słowiński, M.; Lamentowicz, M.; Barabach, J.; Harenda, K.; Zielińska, M.; Robroek, B.; Jassey, V.; Buttler, A.; et al. The Impact of Experimental Temperature and Water Level Manipulation on Carbon Dioxide Release in a Poor Fen in Northern Poland. *Wetlands* **2018**, *38*, 551–563. [CrossRef]

3. Rastogi, A.; Stróżecki, M.; Kalaji, H.M.; Łucόw, D.; Lamentowicz, M.; Juszczak, R. Impact of warming and reduced precipitation on photosynthetic and remote sensing properties of peatland vegetation. *Environ. Exp. Bot.* **2019**, *160*, 71–80. [CrossRef]

4. Loisel, J.; Gallego-Sala, A.V.; Amesbury, M.J.; Magnan, G.; Anshari, G.; Beilman, D.W.; Benavides, J.C.; Blewett, J.; Camill, P.; Charman, D.J.; et al. Expert assessment of future vulnerability of the global peatland carbon sink. *Nat. Clim. Chang.* **2021**, *11*, 70–77. [CrossRef]

5. Belyea, L.R. Nonlinear dynamics of peatlands and potential feedbacks on the climate system. In *Geophysical Monograph Series*; Baird, A.J., Belyea, L.R., Comas, X., Reeve, A.S., Slater, L.D., Eds.; American Geophysical Union: Washington, DC, USA, 2013; pp. 5–18. ISBN 978-1-118-66666-1.

6. Wang, R.; Gamon, J.A. Remote sensing of terrestrial plant biodiversity. *Remote Sens. Environ.* **2019**, *231*, 111218. [CrossRef]

7. Chasmer, L.; Mahoney, C.; Millard, K.; Nelson, K.; Peters, D.; Merchant, M.; Hopkinson, C.; Brisco, B.; Niemann, O.; Montgomery, J.; et al. Remote Sensing of Boreal Wetlands 2: Methods for Evaluating Boreal Wetland Ecosystem State and Drivers of Change. *Remote Sens.* **2020**, *12*, 1321. [CrossRef]

8. Xue, J.; Su, B. Significant Remote Sensing Vegetation Indices: A Review of Developments and Applications. *J. Sens.* **2017**, *2017*, 1353691. [CrossRef]

9. Sishodia, R.P.; Ray, R.L.; Singh, S.K. Applications of Remote Sensing in Precision Agriculture: A Review. *Remote Sens.* **2020**, *12*, 3136. [CrossRef]

10. Badgley, G.; Field, C.B.; Berry, J.A. Canopy near-infrared reflectance and terrestrial photosynthesis. *Sci. Adv.* **2017**, *3*, e1602244. [CrossRef]

11. Meroni, M.; Rossini, M.; Guanter, L.; Alonso, L.; Rascher, U.; Colombo, R.; Moreno, J. Remote sensing of solar-induced chlorophyll fluorescence: Review of methods and applications. *Remote Sens. Environ.* **2009**, *113*, 2037–2051. [CrossRef]

12. Bandopadhyay, S.; Rastogi, A.; Juszczak, R. Review of top-of-canopy sun-induced fluorescence (SIF) studies from ground, uav, airborne to spaceborne observations. *Sensors* **2020**, *20*, 1144. [CrossRef] [PubMed]

13. Yang, P.; van der Tol, C.; Campbell, P.K.E.; Middleton, E.M. Fluorescence Correction Vegetation Index (FCVI): A physically based reflectance index to separate physiological and non-physiological information in far-red sun-induced chlorophyll fluorescence. *Remote Sens. Environ.* **2020**, *240*, 111676. [CrossRef]

14. Harris, A.; Charnock, R.; Lucas, R.M. Hyperspectral Remote Sensing of Peatland Floristic Gradients. *Remote Sens. Environ.* **2015**, *162*, 99–111. [CrossRef]

15. Kalacska, M.; Lalonde, M.; Moore, T. Estimation of foliar chlorophyll and nitrogen content in an ombrotrophic bog from hyperspectral data: Scaling from leaf to image. *Remote Sens. Environ.* **2015**, *169*, 270–279. [CrossRef]

16. McPartland, M.Y.; Falkowski, M.J.; Reinhardt, J.R.; Kane, E.S.; Kolka, R.; Turetsky, M.R.; Douglas, T.A.; Anderson, J.; Edwards, J.D.; Palik, B.; et al. Characterizing Boreal Peatland Plant Composition and Species Diversity with Hyperspectral Remote Sensing. *Remote Sens.* **2019**, *11*, 1685. [CrossRef]

17. Granlund, L.; Vesakoski, V.; Sallinen, A.; Kolari, T.H.M.; Wolff, F.; Tahvanainen, T. Recent Lateral Expansion of Sphagnum Bogs Over Central Fen Areas of Boreal Aapa Mire Complexes. *Ecosystems* **2021**. [CrossRef]

18. Górecki, K.; Rastogi, A.; Stróżecki, M.; Gąbka, M.; Lamentowicz, M.; Łucόw, D.; Kayzer, D.; Juszczak, R. Water table depth, experimental warming, and reduced precipitation impact on litter decomposition in a temperate Sphagnum-peatland. *Sci. Total Environ.* **2021**, *771*, 145452. [CrossRef]

19. Bréda, N.J.J. Leaf area index S. In *Encyclopedia of Ecology*; Brian, E.F., Ed.; Academic Press: Oxford, UK, 2008; pp. 2148–2154.

20. Van der Tol, C.; Rossini, M.; Cogliati, S.; Verhoef, W.; Colombo, R.; Rascher, U.; Mohammed, G. A model and measurement comparison of diurnal cycles of sun-induced chlorophyll fluorescence of crops. *Remote Sens. Environ.* **2016**, *186*, 663–677. [CrossRef]

21. Celesti, M.; van der Tol, C.; Cogliati, S.; Panigada, C.; Yang, P.; Pinto, F.; Rascher, U.; Miglietta, F.; Colombo, R.; Rossini, M. Exploring the physiological information of Sun-induced chlorophyll fluorescence through radiative transfer model inversion. *Remote Sens. Environ.* **2018**, *215*, 97–108. [CrossRef]

22. Shan, N.; Zhang, Y.; Chen, J.M.; Ju, W.; Migliavacca, M.; Peñuelas, J.; Yang, X.; Zhang, Z.; Nelson, J.A.; Goulas, Y. A model for estimating transpiration from remotely sensed solar-induced chlorophyll fluorescence. *Remote Sens. Environ.* **2021**, *252*, 112134. [CrossRef]

23. Yang, P.; Prikaziuk, E.; Verhoef, W.; van der Tol, C. SCOPE 2.0: A model to simulate vegetated land surface fluxes and satellite signals. *Geosci. Model Dev.* **2021**, *14*, 4697–4712. [CrossRef]

24. Pacheco-Labrador, J.; El-Madany, T.S.; van der Tol, C.; Martin, M.P.; Gonzalez-Cascon, R.; Perez-Priego, O.; Guan, J.; Moreno, G.; Carrara, A.; Reichstein, M.; et al. senSCOPE: Modeling mixed canopies combining green and brown senesced leaves. Evaluation in a Mediterranean Grassland. *Remote Sens. Environ.* **2021**, *257*, 112352. [CrossRef]

25. De Cannière, S.; Herbst, M.; Vereecken, H.; Defourny, P.; Jonard, F. Constraining water limitation of photosynthesis in a crop growth model with sun-induced chlorophyll fluorescence. *Remote Sens. Environ.* **2021**, *267*, 112722. [CrossRef]

26. Bandopadhyay, S.; Rastogi, A.; Rascher, U.; Rademske, P.; Schickling, A.; Cogliati, S.; Julitta, T.; Mac Arthur, A.; Hueni, A.; Tomelleri, E.; et al. Hyplant-derived Sun-Induced Fluorescence-A new opportunity to disentangle complex vegetation signals from diverse vegetation types. *Remote Sens.* **2019**, *11*, 1691. [CrossRef]

27. Mac Arthur, A.; Robinson, I.; Hagdorn, M.; Wood, J.; Kershaw, R.; Taylor, R. Piccolo spectrometer system for reflectance and fluorescence measurement from mobile and fixed platforms. In Proceedings of the Innovative Optical Tools for Proximal Sensing of Ecophysiological Processes (OPTIMISE), Vienna, Austria, 23–28 April 2017.

28. Alonso, L.; Gómez-Chova, L.; Vila-Francés, J.; Amorós-López, J.; Guanter, L.; Calpe, J.; Moreno, J. Improved fraunhofer line discrimination method for vegetation fluorescence quantification. *IEEE Geosci. Remote Sens. Lett.* **2008**, *5*, 620–624. [CrossRef]

29. Rouse, J.W.; Haas, R.H.; Schell, J.A.; Deering, D.W. Monitoring vegetation systems in the Great Plains with ERTS. *NASA Spec. Publ.* **1974**, *351*, 309.

30. Liu, H.Q.; Huete, A.R. A feedback based modification of the NDVI to minimize canopy background and atmospheric noise. *IEEE Trans. Geosci. Remote Sens.* **1995**, *33*, 457–465. [CrossRef]

31. Rastogi, A.; Bandopadhyay, S.; Strózecki, M.; Juszczak, R. Monitoring the impact of environmental manipulation on peatland surface by simple remote sensing indices. *ITM Web Conf.* **2018**, *23*, 00030. [CrossRef]

32. Van der Tol, C.; Vilfan, N.; Dauwe, D.; Cendrero-Mateo, M.P.; Yang, P.Q. The scattering and reabsorption of red and near-infrared chlorophyll fluorescence in the models Fluspect and SCOPE. *Remote Sens. Environ.* **2019**, *232*, 111292. [CrossRef]

33. Pope, G.; Treitz, P. Leaf area index (LAI) estimation in boreal mixedwood forest of Ontario, Canada using light detection and ranging (LiDAR) and WorldView-2 imagery. *Remote Sens.* **2013**, *5*, 5040–5063. [CrossRef]

34. Räsänen, A.; Juutinen, S.; Kalacska, M.; Aurela, M.; Heikkinen, P.; Mäenpää, K.; Rimali, A.; Virtanen, T. Peatland leaf-area index and biomass estimation with ultra-high resolution remote sensing. *GIScience Remote Sens.* **2020**, *57*, 943–964. [CrossRef]

35. Antala, M.; Juszczak, R.; van der Tol, C.; Rastogi, A. Impact of climate change-induced alterations in peatland vegetation phenology and composition on carbon balance. *Sci. Total Environ.* **2022**, *827*, 154294. [CrossRef] [PubMed]

36. Bandopadhyay, S.; Rastogi, A.; Cogliati, S.; Rascher, U.; Gąbka, M.; Juszczak, R. Can Vegetation Indices Serve as Proxies for Potential Sun-Induced Fluorescence (SIF)? A Fuzzy Simulation Approach on Airborne Imaging Spectroscopy Data. *Remote Sens.* **2021**, *13*, 2545. [CrossRef]

37. Tesfaye, A.A.; Awoke, B.G. Evaluation of the saturation property of vegetation indices derived from sentinel-2 in mixed crop-forest ecosystem. *Spat. Inf. Res.* **2021**, *29*, 109–121. [CrossRef]

38. Liu, L.; Yang, X.; Gong, F.; Su, Y.; Huang, G.; Chen, X. The Novel Microwave Temperature Vegetation Drought Index (MTVDI) Captures Canopy Seasonality across Amazonian Tropical Evergreen Forests. *Remote Sens.* **2021**, *13*, 339. [CrossRef]

39. Camps-Valls, G.; Campos-Taberner, M.; Moreno-Martínez, A.; Walther, S.; Duveiller, G.; Cescatti, A.; Mahecha, M.D.; Muñoz-Marí, J.; García-Haro, F.J.; Guanter, L.; et al. A unified vegetation index for quantifying the terrestrial biosphere. *Sci. Adv.* **2021**, *7*, eabc7447. [CrossRef] [PubMed]

40. Mishra, K.B.; Mishra, A.; Kubásek, J.; Urban, O.; Heyer, A.G. Low temperature induced modulation of photosynthetic induction in non-acclimated and cold-acclimated Arabidopsis thaliana: Chlorophyll a fluorescence and gas-exchange measurements. *Photosynth. Res.* **2019**, *139*, 123–143. [CrossRef]